Exploring interacting topological insulator in the extended Su-Schrieffer-Heeger model

Xiaofan Zhou [1,2], Jian-Song Pan [3,4,*] and Suotang Jia[1,2]

[1]*State Key Laboratory of Quantum Optics and Quantum Optics Devices, Institute of Laser spectroscopy, Shanxi University, Taiyuan 030006, China*

[2]*Collaborative Innovation Center of Extreme Optics, Shanxi University, Taiyuan 030006, China*

[3]*College of Physics, Sichuan University, Chengdu 610065, China*

[4]*Key Laboratory of High Energy Density Physics and Technology of Ministry of Education, Sichuan University, Chengdu 610065, China*

(Received 5 August 2022; revised 1 February 2023; accepted 3 February 2023; published 14 February 2023)

Exploring topological phases in interacting systems is a challenging task. We investigate many-body topological physics of interacting fermions in an extended Su-Schrieffer-Heeger (SSH) model, which extends the two sublattices of the SSH model into four sublattices and thus is dubbed the SSH4 model, based on the density-matrix renormalization-group numerical method. The interaction-driven phase transition from the topological insulator phase to the charge density wave (CDW) phase can be identified by analyzing the variations of the entanglement spectrum, entanglement entropies, energy gaps, CDW order parameter, and fidelity. We map the global phase diagram of the many-body ground state, which contains nontrivial topological insulator, trivial insulator, and CDW phases, respectively. In contrast to the interacting SSH model, in which the phase transitions to the CDW phase are argued to be first-order phase transitions, the phase transitions between the CDW phase and topologically trivial or nontrivial phases are shown to be continuous phase transitions. Finally, we also show the phase diagram of the interacting spinful SSH4 model, where the attractive (repulsive) on-site spin interaction amplifies (suppresses) the CDW phase. The models analyzed here can be implemented with ultracold atoms on optical superlattices.

DOI: 10.1103/PhysRevB.107.054105

I. INTRODUCTION

Understanding the topological properties of band insulators and interacting topological insulators is one of the most fundamental and challenging tasks in the studies of condensed matter materials and ultracold atomic gases [1–8]. As a highly controllable and disorder-free system, ultracold atoms in optical lattices provide a powerful platform for quantum simulation of topological states of matter [6–8]. One of the most basic and easiest models in describing band topology is the celebrated Su-Schrieffer-Heeger (SSH) model [9], which has been experimentally implemented with ultracold atoms in one-dimensional (1D) dimerized optical superlattices [10–14].

The SSH model describes noninteracting quantum particles hopping in a 1D lattice with alternating hopping coefficients. Varying the hopping ratio, a topological trivial phase or nontrivial phase appears, depending on whether the hopping term at the end of the SSH model is strong or weak [15]. For a noninteracting topological insulator, edge degeneracy comes directly from the zero-energy edge mode, which is protected by the topological invariants of the bulk crystal through the bulk-edge correspondence. After considering the interaction, the SSH model exhibits a rich phase diagram [16–23] and interesting topological bound states [24], where the single-particle picture is not applicable.

On the other hand, stimulated by experimental progress, many variations and extensions of the SSH model have been proposed and explored, such as the driven SSH model [25,26], SSH model with long-range hopping [27–31], two-leg SSH model [32], Creutz ladder model [33–36], and extended SSH model [37]. One typical extended example is to change the site period of the unit cell from 2 to 4; thus one can transform the standard SSH model into the considerably richer SSH4 model with four hopping coefficients [37]. The wider parameter space of the SSH4 model is useful for studying topological properties of the system with higher dimensions including synthetic dimensions [38–42]. The SSH4 model has chiral symmetry and belongs to the same topological class as the SSH model, and the winding number can characterize its band topology [37]. With open boundary conditions, there exist topological edge states at the boundary of the system [43]. For a SSH4 model with infinite sites, the topological trivial and nontrivial phases are determined by the tunneling ratio. So far, the single-particle topological characterizations of SSH4 have been investigated clearly [37,44,45]. However, to the best of our knowledge, a detailed study of the interacting SSH4 model is still lacking.

In this paper, we investigate interacting topological properties of spinless and spin-1/2 SSH4 models in 1D optical superlattices, based on the density-matrix renormalization-group (DMRG) numerical method [46,47]. For the interacting SSH4 model, the topological invariant and classification of interacting topological insulator (TI) become $\mathbb{Z}_4$, which are different from the single-particle TI classified with the $\mathbb{Z}$ group. The nearest-neighbor interaction can drive the TI

*panjsong@scu.edu.cn

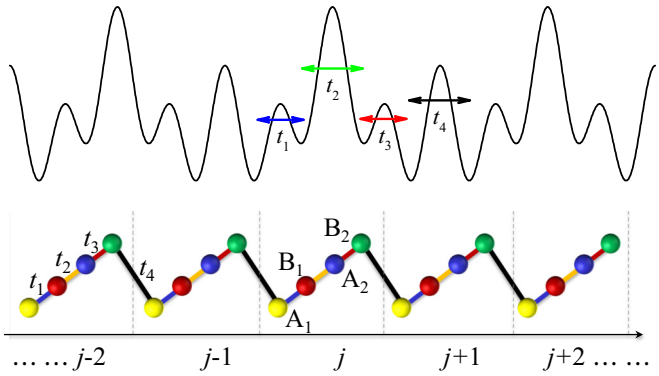

FIG. 1. A sketch of the SSH4 model. Three superposed optical lattices with lattice constants $a/2$, a, and $2a$ effectively realize an SSH4 model. This model exhibits four sites per unit cell with four tunnelings, which can be tuned independently by varying the three lattice strengths and relative phase between the lattices.

and the topologically trivial insulator phases to the charge density wave (CDW) phase, which is characterized with the entanglement spectrum, entanglement entropies, energy gaps, and CDW order parameter. We numerically work out the many-body phase diagrams and show the typical features of the quantum phases that appear. Although the phase diagram is similar to that of the interacting SSH model, we find that the phase transitions to the CDW phase are continuous phase transitions, unlike those in the SSH model, which are argued to be first-order phase transitions based on variational study [48]. The central charges at the phase boundaries between the CDW phase and the TI and trivial insulator phase are shown to be 2 and 1, respectively. Furthermore, we analyze the ground states of the interacting spinful SSH4 model. This analysis shows that the repulsive on-site interaction of the spin-1/2 SSH4 model can enhance the TI phase and suppress the CDW phase, but the attractive on-site interaction plays the opposite role. Our results may stimulate an avenue for simulating interacting fermionic topological phases using cold atoms in optical lattices.

II. MODEL AND HAMILTONIAN

In a cold-atom experiment, three superposed optical lattices with lattice constants $a/2$, a, and $2a$ effectively realize an SSH4 model, as shown in Fig. 1. The three optical lattices may be obtained from a single laser working at $\lambda_{\text{laser}} = 1064$ nm. The $a/2$ optical lattice can be obtained by retroreflecting the frequency-doubled laser, with $a = \lambda_{\text{laser}}/2$. The a lattice may be obtained by retroreflecting the laser λ_{laser}. The lattice at $2a$ may be obtained by crossing two λ_{laser} beams with a small angle [37]. This superlattice exhibits four sites per unit cell (see Fig. 1) and hence is called the SSH4 model. The tight-binding interacting SSH4 Hamiltonian can be written as

$$H = \sum_{j=1}^{L/4} [t_1 \hat{c}^\dagger_{4j-3}\hat{c}_{4j-2} + t_2 \hat{c}^\dagger_{4j-2}\hat{c}_{4j-1} + t_3 \hat{c}^\dagger_{4j-1}\hat{c}_{4j} + t_4 \hat{c}^\dagger_{4j}\hat{c}_{4j+1} + \text{H.c.}] + V \sum_{j}^{L} \hat{n}_j \hat{n}_{j+1}, \quad (1)$$

where $\hat{c}_j$ ($\hat{c}^\dagger_j$) are fermionic annihilation (creation) operators of the jth site, $\hat{n}_j = \hat{c}^\dagger_j \hat{c}_j$, t_n are the tunneling rates, and V measures the nearest-neighbor density-density interaction. In this configuration, $t_1 = t_3$, but t_2 and t_4 can be tuned independently by varying the three lattice strengths and relative phase between the three lattices.

For single-particle items of Hamiltonian (1), the time-reversal, particle-hole, and chiral symmetries exist; then the topological insulator belongs to the symmetry class BDI of the Altland-Zirnbauer classification and is characterized by a $\mathbb{Z}$ invariant [4,49–51]. When $t_1 = t_3$ and $t_2 = t_4$, the SSH4 model reduces to the common SSH model. The SSH4 model has four bands with more midgap states located inside the three gaps. However, only the zero-energy state is protected by the chiral symmetry and associated with the band topology. Thus the winding number is defined to identify the property of the two negative (or positive) energy bands, which all contribute to its value. The winding number $w = 1$ when $|t_1 t_3| < |t_2 t_4|$, and $w = 0$ when $|t_1 t_3| > |t_2 t_4|$. In the presence of weak interaction V, the topological invariant becomes $\mathbb{Z}_4$ [52]. In the following, we focus on the two negative topology bands with zero-energy states, which corresponds to the half-filling occupation, i.e., $N/L = 0.5$, with the atom number N and lattice length L.

The Hamiltonian (1) shows the spinless SSH4 model. In a cold-atom experiment, the hyperfine states of the atoms usually can be treated as components of spin. After considering the two hyperfine states, we can get the spin-1/2 SSH4 Hamiltonian, which can be written as

$$H = \sum_{j=1,\sigma}^{L/4} [t_1 \hat{c}^\dagger_{4j-3,\sigma}\hat{c}_{4j-2,\sigma} + t_2 \hat{c}^\dagger_{4j-2,\sigma}\hat{c}_{4j-1,\sigma} + t_3 \hat{c}^\dagger_{4j-1,\sigma}\hat{c}_{4j,\sigma} + t_4 \hat{c}^\dagger_{4j,\sigma}\hat{c}_{4j+1,\sigma} + \text{H.c.}] + V \sum_{j} \hat{n}_j \hat{n}_{j+1} + U \sum_{j} \hat{n}_{j,\uparrow}\hat{n}_{j,\downarrow}, \quad (2)$$

where σ presents the spin (spin up and spin down, $\uparrow, \downarrow$) for a spin-1/2 fermion and U is the on-site interaction strength between opposite spins due to s-wave scattering with $\hat{n}_j = \sum_\sigma \hat{c}^\dagger_{j,\sigma}\hat{c}_{j,\sigma}$ being the number operator. With the spin degree of freedom, the model exhibits eight energy bands. The topological insulator is presented at the filling $N/L = 1$.

In order to quantitatively reveal the SSH4 models, we will perform the DMRG numerical method with lattice length up to $L = 320$ for the spinless SSH4 model and $L = 128$ for the spin-1/2 SSH4 model, for which we retain 400 truncated states per DMRG block and perform 30 sweeps with acceptable truncation errors [53].

III. ORDER PARAMETERS

The strongly correlated topological properties can be well described by the degeneracy in the entanglement spectrum of the ground state, entanglement entropy, and excited energy gap. The system is topological nontrivial if the entanglement spectrum is degenerate since the entanglement spectrum is associated with the energy spectrum of edge excitations [16, 54–59]. The entanglement spectrum is defined as a

logarithmic rescaling of the Schmidt values [54]

$$\xi_i = -\ln(\rho_i), \tag{3}$$

with ρ_i being the eigenvalue of the reduced density matrix $\hat{\rho}_l = \mathrm{Tr}_{L-l}|\psi\rangle\langle\psi|$, where $|\psi\rangle$ is the ground-state wave function of Hamiltonian (1) and l is the length of the left block for a specific bipartition. The quantum criticality of the interaction-driven topological phase transition can be characterized with the von Neumann entropy [59–64]

$$S_{\mathrm{vN}} = -\mathrm{Tr}_l[\hat{\rho}_l \ln \hat{\rho}_l], \tag{4}$$

with $l = L/2$ being the half part of the lattice. It is believed that the property underlying the long-range correlations is entanglement [65] and, on the other hand, the correlation length becomes divergent at the critical point of the continuous phase transition [66]. The divergence of the von Neumann entropy at the critical point thus indicates a continuous transition [57]. Besides, the von Neumann entropy also reveals the central charge of the conformal field theory underlying the critical behavior, which generally determines the effective field theory and reflects the universality class of the phase transition [67]. For a critical system under periodic boundary conditions, the von Neumann entropy of a subchain of length l scales as

$$S_{\mathrm{vN}}(l) = \frac{c}{3}\ln\left[\sin\frac{\pi l}{L}\right] + \mathrm{const}, \tag{5}$$

in which the slope at large distance gives the central charge c of the conformal field theory [67–70]. The formula for the case under open boundary conditions is obtained by replacing 3 by 6.

One also can use the fidelity of the wave function of the ground states to identify the phase transition, which can be defined as the modulus of the overlap between two states (ψ', ψ) [71]

$$F(\psi', \psi) = |\langle\psi'|\psi\rangle|, \tag{6}$$

where $|\psi\rangle$ and $|\psi'\rangle$ are the input and output states, respectively, and both of them are normalized. The topological ground state of the extended SSH model under periodic boundary conditions is nondegenerate and separated from the first excited state by a finite gap, which closes and reopens across a topological phase transition. The excited energy gap is defined as

$$\Delta_e = E_e^p(N) - E_g^p(N), \tag{7}$$

where $E_e^p(N)$ $[E_g^p(N)]$ is the first excited state (ground-state) energy of N atoms under periodic boundary conditions. As we all know, the nearest-neighbor interaction V can induce the CDW phase, in which the CDW order parameters can be defined as

$$C = \frac{1}{L}\sum_{i=1}^{L}(-1)^i\langle\hat{n}_i\rangle. \tag{8}$$

For a TI under open boundary conditions, the presence of localized density of the edge mode is a typical feature. The density distribution of the edge modes can be calculated as

$$\langle\Delta\hat{n}_j\rangle = \langle\hat{n}_j(N+1)\rangle - \langle\hat{n}_j(N)\rangle, \tag{9}$$

with $\langle\hat{n}_j(N)\rangle$ being the density distribution for N atoms under open boundary conditions.

IV. MANY-BODY QUANTUM PHASES

A. Spinless SSH4

We first characterize the many-body properties of the spinless SSH4 Hamiltonian (1). Based on the experimental setup, we here fixed $t_1 = t_3 = t_4 = 1$ and vary t_2. When increasing t_2 from 0 to 2 in the absence of interaction, the phase is a trivial band insulator (BI) when $t_2 < 1$ and a TI when $t_2 > 1$ with critical point $t_2^c = 1$. Here we consider the topological phase transition driven by the nearest-neighbor interaction V for a fixed tunneling, i.e., $t_2 = 1.6$. For zero and weak nearest-neighbor interaction strength V, the lowest entanglement spectrum ξ_i is twofold degenerate for finite lattice size $L = 320$, as shown in Fig. 2(a). However, the ξ_i show different features for noninteracting and weak interaction topological insulators. For the noninteracting topological insulator, some of the high levels of ξ_i show fourfold degeneracy. However, all levels of ξ_i for weak interacting topological insulator are twofold degenerate [see Fig. 2(b)]. Further increasing the interaction strength V, ξ_i is no longer degenerate beyond a critical interaction strength $V_c \sim 4.34$, as shown in Fig. 2(a). The von Neumann entropy S_{vN} also exhibits a sharp peak at around the critical point, as shown in Fig. 2(c). Moreover, the excited energy gap Δ_e under periodic boundary conditions closes at the critical point and then reopens, as shown in Figs. 2(d) and 2(e). In this processing of the phase transition, the CDW order parameter C goes to finite values from zero when V goes beyond the critical strength V_c, as shown in Fig. 2(f). Above all, one can conclude that the nearest-neighbor interaction V drives the TI into the CDW phase through a phase transition.

In the CDW phase, the chiral symmetry protecting the nontrivial topological phase has been spontaneously broken by the CDW order [48]. The ground states of the interacting SSH model are approximately equivalent to that of a noninteracting SSH model plus an additional on-site staggered term in the CDW phase [48]. Hence the phase transitions from the topologically trivial or nontrivial phases to the CDW phase can be classified with Landau's paradigm. Specifically, the local order parameter characterizing the phase transition is the CDW order defined in Eq. (8). Although the CDW phase is a topologically trivial phase, evidenced by the lacking of entanglement-entropy degeneracy, as shown in Fig. 2(a), the phase transition to the CDW phase is not a standard topological phase transition in the common sense, because it can be described with local order parameters and accompanies the spontaneous breaking of symmetries. It is consistent with the transition from the topological band insulator to the antiferromagnetic Mott insulator in the two-dimensional Kane-Mele-Hubbard model [72], which is in the universality class of the three-dimensional XY model that also accompanies spontaneous symmetry breaking [73].

As expected from the previous literature [71], a sharp dip in the curve of the fidelity $|\langle\psi(V)|\psi(V+\delta V)\rangle|$ $(\delta V = 0.02)$ accompanies the emergence of the quantum phase transition, and the dip becomes sharper and sharper as the system size

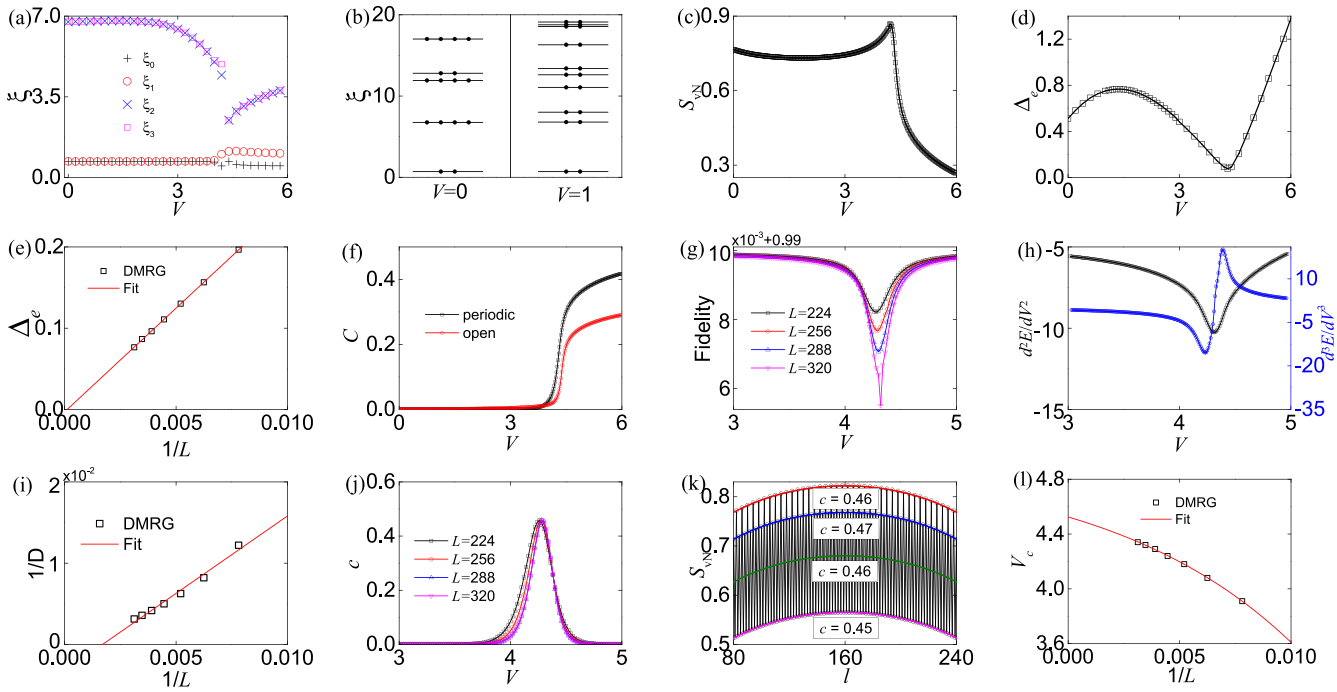

FIG. 2. (a) The lowest four levels in the entanglement spectrum ξ_i ($i = 0, 1, 2, 3$) as a function of the interaction strength V. (b) The 16 lower levels in the entanglement spectrum for two values of $V = 0, 1$. (c) The von Neumann entropy $S_{\rm vN}$ and (d) the excited energy gap Δ_e vs V. (e) The finite-size scaling of the Δ_e at the critical point; the red solid line is a linear fit with $\Delta_e \sim 0$ in the large-L limit. (f) The CDW order parameter C, (g) the fidelity $\langle\psi(V)|\psi(V+\delta V)\rangle$ ($\delta V = 0.02$) of finite lattice lengths, and (h) the derivatives of the ground-state energy d^nE/dV^n ($n = 2, 3$) vs V. (i) The finite-size scaling of the inverse of the peak value of the fourth-order derivative of the ground-state energy (not shown here). (j) The fitting central charge c (note that only at the critical point can c be defined, although we always can fit the formula and obtain a value) as a function of the interaction strength V. (k) The scaling of the von Neumann entropy $S_{\rm vN}(l)$ as a function of subchain l at the critical point. The green line is $S_{\rm vN}(l) = \frac{c}{3}\ln[\sin(\pi l/L)] + \text{const}$ with $c = 0.46$ (extracted from the fitting of the mean values of $S_{\rm vN}$). (l) The finite-size scaling of the critical point for the phase transition between TI and CDW with $t_2 = 1.6$. The critical point $V_c = 4.53$ in the thermodynamic limits. In all panels, we have $t_2 = 1.6$ and $L = 320$ except the finite-size scalings. All panels are under periodic boundary conditions.

increases, as shown in Fig. 2(g). This behavior is associated with the dramatic change in the ground state in the critical regime. It is argued that the phase transition to the CDW phase in the interacting SSH model is a first-order phase transition when the difference between the alternating hopping coefficients is not too large, based on a variational study [48]. In contrast, we find that this transition in the interacting SSH4 model considered here is a continuous (third-order) phase transition, as directly evidenced by the discontinuousness of the third-order derivative of the ground-state energy [see Fig. 2(h)]. Actually, the sharp peak in the entanglement entropy shown in Fig. 2(c) also indicates that the phase transition is continuous. Note that the discontinuousness of the third-order derivative of the ground-state energy does not look so obvious in the figure due to the system size being finite in the numerical calculation, but it obviously shows a sharp jump at around the critical point. As shown in Fig. 2(i), the finite-size scaling indicates that the fourth-order derivative of the ground-state energy moves toward the divergent regime in the thermodynamic limit (the relatively large deviation is due to the fact that the derivatives are calculated with numerical difference order by order). This observation further confirms that the third-order derivative of the energy is not continuous and the CDW phase transition is a third-order phase transition.

At the critical point between the TI and CDW, the energy spectrum is gapless in the thermodynamic limit [i.e., $\Delta_e = 0$; see Fig. 2(e)], and the scaling of the von Neumann entropy $S_{\rm vN}(l) = \frac{c}{3}\ln[\sin(\pi l/L)] + \text{const}$ with a central charge $c = 0.46$, as shown in Figs. 2(j) and 2(k). The critical line is the Luttinger liquid with central charge $c = 0.46$. By using finite-size scaling, we get the critical points of interaction-driven Landau phase transitions between TI and CDW $V_c = 4.53$ when $t_2 = 1.6$ in the thermodynamic limit for the interacting SSH4 model, as shown in Fig. 2(l). We use similar methods to identify the critical points V_c for several t_2.

According to the calculated degeneracy of the entanglement spectrum, entanglement entropy, energy gaps, CDW parameter order, fidelity, and derivatives of the ground-state energy, we can draw the phase diagram in the t_2-V plane, as shown in Fig. 3(a). This phase diagram contains three phases: TI, BI, and CDW. By scaling the von Neumann entropy $S_{\rm vN}(l)$ of the critical lines, we find that the critical line between TI and CDW (BI) is the Luttinger liquid with central charge $c = 0.46$. For large nearest-neighbor interaction strength V, the density profile $\langle\hat{n}_j\rangle$ of the ground state always modulates along real lattice space with a period of 2; the corresponding phase is CDW, as shown in Fig. 3(b). For weak V, the ground state is TI (BI) when $t_2 > 1$ ($t_2 < 1$). The TI not only

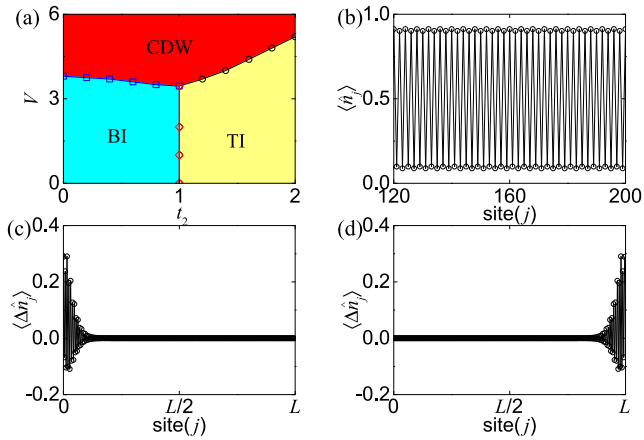

FIG. 3. (a) The phase diagram of the spinless SSH4 Hamiltonian (1) in the t_2-V plane in the thermodynamic limit under periodic boundary conditions, which contains topological insulator (TI), band insulator (BI), and charge density wave (CDW) phases. The critical line between TI and CDW (black line with circles) is the Luttinger liquid with central charge $c = 0.46$. The critical line between TI and BI (red line with diamonds) is the Luttinger liquid with central charge $c = 0.46$. (b) The density profile $\langle \hat{n}_j \rangle$ of the CDW with $t_2 = 1.2$ and $V = 5.0$ under periodic boundary conditions. (c) and (d) The edge-model density distributions $\langle \Delta \hat{n}_j \rangle$ of the twofold degenerate TI with $t_2 = 1.6$ and $V = 2.0$ under open boundary conditions. In (b)–(d), we have $L = 320$ and $N = 160$.

exhibits a twofold degenerate entanglement spectrum but also has a twofold degenerate ground state under open boundary conditions, in which only one edge mode is occupied on one edge side for each degenerate ground state, as shown in Figs. 3(c) and 3(d). For BI, the density profile is uniform (i.e., $\langle \hat{n}_j \rangle = 0.5$), and the entanglement spectrum is almost completely nondegenerate, which are not shown.

B. Spin-1/2 SSH4

Here, we consider the spin-1/2 SSH4 Hamiltonian (2), which contains the on-site interaction. Similarly to Fig. 3, we calculate the entanglement spectrum, entanglement entropy, energy gaps, CDW orders, fidelity, derivatives of the ground-state energy, and central charge, as shown in Fig. 4. Combining with the finite-size scaling, we map out the phase diagram of the spin-1/2 SSH4 model, as shown in Figs. 5(a) and 5(b). For the filling $N/L = 1$, the atoms fully occupy the lower half of the eight energy bands in the BI and TI regimes. The repulsive on-site interaction favors less density on the same site, while the CDW phase has twice the density compared with the uniform BI and TI cases. Therefore repulsive on-site interaction enhances the TI (BI) phases and suppresses the CDW phase. In contrast, the attractive on-site interaction suppresses the TI (BI) phases but enhances the CDW phase.

We would like to note that, in contrast to the spinless case, the interspin nearest-neighbor interaction terms in the spinful case also enhance the CDW phase, even when the

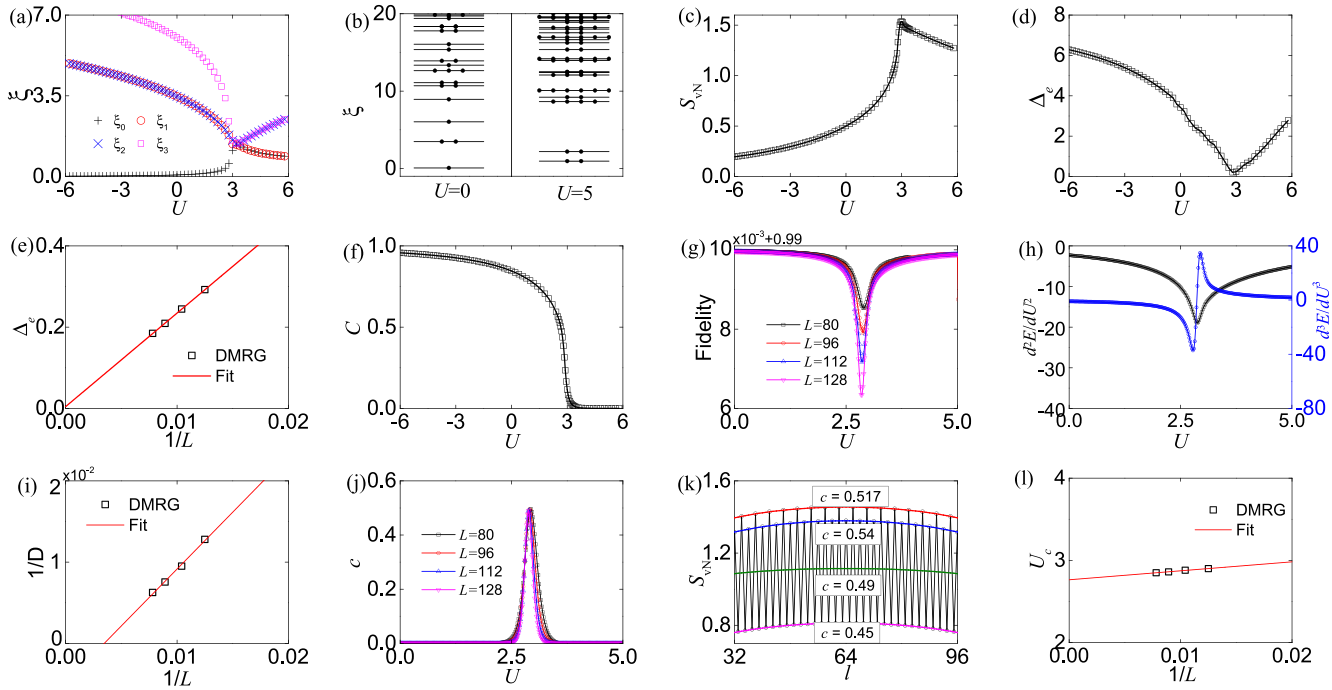

FIG. 4. Similar to Fig. 3. (a) The entanglement spectrum ξ_i vs U. (b) The several lower levels in the entanglement spectrum for two values of $U = 0, 5$. (c) The von Neumann entropy $S_{\rm vN}$ and (d) the excited energy gap Δ_e vs U. (e) The finite-size scaling of the Δ_e at the critical point. (f) The CDW order parameter C, (g) the fidelity $\langle \psi(U) | \psi(U + \delta U) \rangle$ ($\delta U = 0.02$), and (h) the derivatives of the ground-state energy $d^n E/dU^n$ ($n = 2, 3$) vs U. (i) The finite-size scaling of the inverse of the peak value of the fourth-order derivative of the ground-state energy. (j) The fitting central charge c as a function of the interaction strength U. (k) The scaling of the von Neumann entropy $S_{\rm vN}(l)$ as a function of subchain l at the critical point. (l) The finite-size scaling of the critical point for the phase transition between TI and CDW. In all panels, we have $t_2 = 1.6$, $V = 2.0$, and $L = N = 128$ except the finite-size scalings. All panels are under periodic boundary conditions.

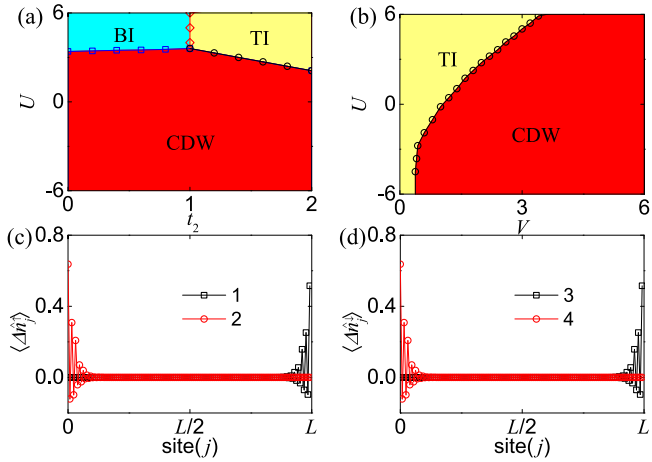

FIG. 5. The phase diagram of the spin-1/2 SSH4 Hamiltonian (2) (a) in the t_2-U plane with $V = 2$ and (b) in the V-U plane with $t_2 = 1.6$ in the thermodynamic limit under periodic boundary conditions. The edge-model density distributions of different spin $\langle \Delta \hat{n}_j^\sigma \rangle$ (c) $\sigma = \uparrow$ and (d) $\sigma = \downarrow$, with $t_2 = 1.6$, $U = 5.0$, $V = 2.0$, and $L = N = 128$ under open boundary conditions. In (c) and (d), the numbers in the figure legends label different degenerate ground states.

on-site interaction is absent. The spinful case thus has a lower critical value of nearest-neighbor interaction for the CDW phase transition. For example, as shown in Fig. 5 (Fig. 3), the spinful (spinless) system already enters (has not entered) the CDW phase when $U = 0$ and $V = 2$ ($V = 2$).

For the TI in the repulsive on-site interaction regime, only the one-component atoms can be localized at one side of the edge. The TI features fourfold degeneracies in the ground state with fourfold localized density distributions at the edge, such as $|\uparrow\rangle$ located at the left edge, $|\uparrow\rangle$ located at the right edge, $|\downarrow\rangle$ located at the left edge, and $|\downarrow\rangle$ located at the right edge, as shown in Figs. 5(c) and 5(d). For the TI in the attractive on-site interaction regime, both the two-component atoms with equal number are localized at one side of the edge. The ground state has twofold degeneracies: One is $|\uparrow + \downarrow\rangle$ located at the left edge, and the other is $|\uparrow + \downarrow\rangle$ located at the right edge.

V. CONCLUSIONS

In conclusion, we have studied theoretically the interacting SSH4 models at half filling using the DMRG method. We find that the nearest-neighbor interaction can drive the TI (BI) phase to the CDW phase. Varying the tunnelings, there exists the topological phase transition between TI and BI. The critical lines of the topological phase transitions correspond to the Luttinger liquids with integer central charges. We have calculated the entanglement spectrum, entanglement entropy, energy gaps, and CDW order parameter, to identify the interaction-driven CDW phase transitions and phase diagrams. The phase transition to the CDW phase driven by interaction is shown to be a continuous phase transition. The central charges at the phase boundaries are fixed. We also have studied the topological properties of the spin-1/2 interacting SSH4 model and find that the repulsive on-site interaction can enhance the TI and suppress the CDW phase. However, the attractive on-site interaction plays the opposite role. We also investigate the edge model of the TIs. In experiment, the entanglement entropy can be measured using quantum interference of many-body twins of ultracold atoms in optical lattices [64]. The CDW phase can be detected by time-of-flight measurements in cold-atom experiments. Our work provides insights into the many-body physics in systems with topological properties and may stimulate the quantum simulation of strongly correlated topological insulators with cold atoms in optical superlattices.

ACKNOWLEDGMENTS

X.Z. and S.J. are supported by the National Key R&D Program of China under Grant No. 2017YFA0304203, the National Natural Science Foundation of China (NSFC) under Grant No. 12004230, and the Research Project Supported by Shanxi Scholarship Council of China and Shanxi (Project No. 1331KSC). J.-S.P. is supported by the NSFC under Grant No. 11904228 and the Science Specialty Program of Sichuan University under Grant No. 2020SCUNL210. Our simulations make use of the ALPSCORE library [74], based on the original Algorithms and Libraries for Physics Simulations (ALPS) project [75].

[1] M. Z. Hasan and C. L. Kane, Colloquium: Topological insulators, Rev. Mod. Phys. **82**, 3045 (2010).
[2] X.-L. Qi and S.-C. Zhang, Topological insulators and superconductors, Rev. Mod. Phys. **83**, 1057 (2011).
[3] A. Bansil, H. Lin, and T. Das, Colloquium: Topological band theory, Rev. Mod. Phys. **88**, 021004 (2016).
[4] C.-K. Chiu, J. C. Y. Teo, A. P. Schnyder, and S. Ryu, Classification of topological quantum matter with symmetries, Rev. Mod. Phys. **88**, 035005 (2016).
[5] N. P. Armitage, E. J. Mele, and A. Vishwanath, Weyl and Dirac semimetals in three-dimensional solids, Rev. Mod. Phys. **90**, 015001 (2018).
[6] N. Goldman, J. C. Budich, and P. Zoller, Topological quantum matter with ultracold gases in optical lattices, Nat. Phys. **12**, 639 (2016).
[7] D.-W. Zhang, Y.-Q. Zhu, Y. X. Zhao, H. Yan, and S.-L. Zhu, Topological quantum matter with cold atoms, Adv. Phys. **67**, 253 (2018).
[8] N. R. Cooper, J. Dalibard, and I. B. Spielman, Topological bands for ultracold atoms, Rev. Mod. Phys. **91**, 015005 (2019).
[9] W. P. Su, J. R. Schrieffer, and A. J. Heeger, Solitons in Polyacetylene, Phys. Rev. Lett. **42**, 1698 (1979).
[10] M. Atala, M. Aidelsburger, J. T. Barreiro, D. Abanin, T. Kitagawa, E. Demler, and I. Bloch, Direct measurement of the Zak phase in topological Bloch bands, Nat. Phys. **9**, 795 (2013).
[11] L. Wang, M. Troyer, and X. Dai, Topological Charge Pumping in a One-Dimensional Optical Lattice, Phys. Rev. Lett. **111**, 026802 (2013).

[12] M. Lohse, C. Schweizer, O. Zilberberg, M. Aidelsburger, and I. Bloch, A Thouless quantum pump with ultracold bosonic atoms in an optical superlattice, Nat. Phys. **12**, 350 (2016).

[13] S. Nakajima, T. Tomita, S. Taie, T. Ichinose, H. Ozawa, L. Wang, M. Troyer, and Y. Takahashi, Topological Thouless pumping of ultracold fermions, Nat. Phys. **12**, 296 (2016).

[14] M. Leder, C. Grossert, L. Sitta, M. Genske, A. Rosch, and M. Weitz, Real-space imaging of a topologically protected edge state with ultracold atoms in an amplitude-chirped optical lattice, Nat. Commun. **7**, 13112 (2016).

[15] S. Q. Shen, *Topological Insulators: Dirac Equation in Condensed Matters* (Springer, New York, 2012).

[16] T. Yoshida, R. Peters, S. Fujimoto, and N. Kawakami, Characterization of a Topological Mott Insulator in One Dimension, Phys. Rev. Lett. **112**, 196404 (2014).

[17] J. Sirker, M. Maiti, N. P. Konstantinidis, and N. Sedlmayr, Boundary fidelity and entanglement in the symmetry protected topological phase of the SSH model, J. Stat. Mech. (2014) P10032.

[18] D. Wang, S. Xu, Y. Wang, and C. Wu, Detecting edge degeneracy in interacting topological insulators through entanglement entropy, Phys. Rev. B **91**, 115118 (2015).

[19] M. Di Liberto, A. Recati, I. Carusotto, and C. Menotti, Two-body physics in the Su-Schrieffer-Heeger model, Phys. Rev. A **94**, 062704 (2016).

[20] B.-T. Ye, L.-Z. Mu, and H. Fan, Entanglement spectrum of Su-Schrieffer-Heeger-Hubbard model, Phys. Rev. B **94**, 165167 (2016).

[21] K. Meichanetzidis, J. Eisert, M. Cirio, V. Lahtinen, and J. K. Pachos, Diagnosing Topological Edge States via Entanglement Monogamy, Phys. Rev. Lett. **116**, 130501 (2016).

[22] A. M. Marques and R. G. Dias, Multihole edge states in Su-Schrieffer-Heeger chains with interactions, Phys. Rev. B **95**, 115443 (2017).

[23] Y. Kuno, Phase structure of the interacting Su-Schrieffer-Heeger model and the relationship with the Gross-Neveu model on lattice, Phys. Rev. B **99**, 064105 (2019).

[24] A. M. Marques and R. G. Dias, Topological bound states in interacting Su–Schrieffer–Heeger rings, J. Phys.: Condens. Matter **30**, 305601 (2018).

[25] A. Gómez-León and G. Platero, Floquet-Bloch Theory and Topology in Periodically Driven Lattices, Phys. Rev. Lett. **110**, 200403 (2013).

[26] V. Dal Lago, M. Atala, and L. E. F. F. Torres, Floquet topological transitions in a driven one-dimensional topological insulator, Phys. Rev. A **92**, 023624 (2015).

[27] L. Li, Z. Xu, and S. Chen, Topological phases of generalized Su-Schrieffer-Heeger models, Phys. Rev. B **89**, 085111 (2014).

[28] F. A. An, E. J. Meier, and B. Gadway, Engineering a Flux-Dependent Mobility Edge in Disordered Zigzag Chains, Phys. Rev. X **8**, 031045 (2018).

[29] B. Perez-Gonzalez, M. Bello, A. Gomez-Leon, and G. Platero, Interplay between long-range hopping and disorder in topological systems, Phys. Rev. B **99**, 035146 (2019).

[30] N. Ahmadi, J. Abouie, and D. Baeriswyl, Topological and nontopological features of generalized Su-Schrieffer-Heeger models, Phys. Rev. B **101**, 195117 (2020).

[31] R. R. Kumar, N. Roy, Y. R. Kartik, S. Rahul, and S. Sarkar, Topological phase transition at quantum criticality, arXiv:2112.02485.

[32] S.-L. Zhang and Q. Zhou, Two-leg Su-Schrieffer-Heeger chain with glide reflection symmetry, Phys. Rev. A **95**, 061601(R) (2017).

[33] N. Sun and L.-K. Lim, Quantum charge pumps with topological phases in a Creutz ladder, Phys. Rev. B **96**, 035139 (2017).

[34] J. Jünemann, A. Piga, S.-J. Ran, M. Lewenstein, M. Rizzi, and A. Bermudez, Exploring Interacting Topological Insulators with Ultracold Atoms: The Synthetic Creutz-Hubbard Model, Phys. Rev. X **7**, 031057 (2017).

[35] J. H. Kang, J. H. Han, and Y. Shin, Realization of a Cross-Linked Chiral Ladder with Neutral Fermions in a 1D Optical Lattice by Orbital-Momentum Coupling, Phys. Rev. Lett. **121**, 150403 (2018).

[36] J. Y. He, R. Mao, H. Cai, J.-X. Zhang, Y. Li, L. Yuan, S.-Y. Zhu, and D.-W. Wang, Flat-Band Localization in Creutz Superradiance Lattices, Phys. Rev. Lett. **126**, 103601 (2021).

[37] M. Maffei, A. Dauphin, F. Cardano, M. Lewenstein, and P. Massignan, Topological characterization of chiral models through their long time dynamics, New J. Phys. **20**, 013023 (2018).

[38] A. Celi, P. Massignan, J. Ruseckas, N. Goldman, I. B. Spielman, G. Juzeliūnas, and M. Lewenstein, Synthetic Gauge Fields in Synthetic Dimensions, Phys. Rev. Lett. **112**, 043001 (2014).

[39] H. M. Price, O. Zilberberg, T. Ozawa, I. Carusotto, and N. Goldman, Four-Dimensional Quantum Hall Effect with Ultracold Atoms, Phys. Rev. Lett. **115**, 195303 (2015).

[40] M. Mancini, G. Pagano, G. Cappellini, L. Livi, M. Rider, J. Catani, C. Sias, P. Zoller, M. Inguscio, M. Dalmonte, and L. Fallani, Observation of chiral edge states with neutral fermions in synthetic Hall ribbons, Science **349**, 1510 (2015).

[41] B. K. Stuhl, H.-I. Lu, L. M. Aycock, D. Genkina, and I. B. Spielman, Visualizing edge states with an atomic Bose gas in the quantum Hall regime, Science **349**, 1514 (2015).

[42] E. Lustig, S. Weimann, Y. Plotnik, Y. Lumer, M. A. Bandres, A. Szameit, and M. Segev, Photonic topological insulator in synthetic dimensions, Nature (London) **567**, 356 (2019).

[43] A. M. Marques and R. G. Dias, Analytical solution of open crystalline linear 1D tight-binding models, J. Phys. A: Math. Theor. **53**, 075303 (2020).

[44] D. Xie, W. Gou, T. Xiao, B. Gadway, and B. Yan, Topological characterizations of an extended Su-Schrieffer-Heeger model, npj Quantum Inf. **5**, 55 (2019).

[45] Y. He and C.-C. Chien, Non-Hermitian generalizations of extended Su-Schrieffer-Heeger models, J. Phys.: Condens. Matter **33**, 085501 (2021).

[46] S. R. White, Density Matrix Formulation for Quantum Renormalization Groups, Phys. Rev. Lett. **69**, 2863 (1992).

[47] U. Schollwöck, The density-matrix renormalization group, Rev. Mod. Phys. **77**, 259 (2005).

[48] M. Yahyavi, L. Saleem, and B. Hetényi, Variational study of the interacting, spinless Su-Schrieffer-Heeger model, J. Phys.: Condens. Matter **30**, 445602 (2018).

[49] A. Altland and M. R. Zirnbauer, Nonstandard symmetry classes in mesoscopic normal-superconducting hybrid structures, Phys. Rev. B **55**, 1142 (1997).

[50] A. P. Schnyder, S. Ryu, A. Furusaki, and A. W. W. Ludwig, Classification of topological insulators and superconductors in three spatial dimensions, Phys. Rev. B **78**, 195125 (2008).

[51] A. W. W. Ludwig, Topological phases: classification of topological insulators and superconductors of non-interacting fermions, and beyond, Phys. Scr. **2016**, 014001 (2016).

[52] T. Morimoto, A. Furusaki, and C. Mudry, Breakdown of the topological classification Z for gapped phases of noninteracting fermions by quartic interactions, Phys. Rev. B **92**, 125104 (2015).

[53] Although the truncation errors (the sum of all discarded eigenvalues in the reduced density matrix) for the excited states are far larger than those for the ground states, the maximum truncation errors are basically smaller than 10^{-6} and are acceptable. In the spinless model with lattice length $L = 320$, the ground states have truncation errors smaller than 10^{-31}. The excited states even still have truncation errors smaller than 10^{-11}. For the spinful model with lattice length $L = 128$, the truncation errors for the ground state are smaller than 10^{-9}. Even for the excited states in the spinful model, we still have truncation errors smaller than 10^{-6}.

[54] H. Li and F. D. M. Haldane, Entanglement Spectrum as a Generalization of Entanglement Entropy: Identification of Topological Order in Non-Abelian Fractional Quantum Hall Effect States, Phys. Rev. Lett. **101**, 010504 (2008).

[55] J.-Z. Zhao, S.-J. Hu, and P. Zhang, Symmetry-Protected Topological Phase in a One-Dimensional Correlated Bosonic Model with a Synthetic Spin-Orbit Coupling, Phys. Rev. Lett. **115**, 195302 (2015).

[56] A. M. Turner, F. Pollmann, and E. Berg, Topological phases of one-dimensional fermions: An entanglement point of view, Phys. Rev. B **83**, 075102 (2011).

[57] F. Pollmann, A. M. Turner, E. Berg, and M. Oshikawa, Entanglement spectrum of a topological phase in one dimension, Phys. Rev. B **81**, 064439 (2010).

[58] L. Fidkowski, Entanglement Spectrum of Topological Insulators and Superconductors, Phys. Rev. Lett. **104**, 130502 (2010).

[59] S. T. Flammia, A. Hamma, T. L. Hughes, and X.-G. Wen, Topological Entanglement Rényi Entropy and Reduced Density Matrix Structure, Phys. Rev. Lett. **103**, 261601 (2009).

[60] M. B. Hastings, I. González, A. B. Kallin, and R. G. Melko, Measuring Rényi Entanglement Entropy in Quantum Monte Carlo Simulations, Phys. Rev. Lett. **104**, 157201 (2010).

[61] A. J. Daley, H. Pichler, J. Schachenmayer, and P. Zoller, Measuring Entanglement Growth in Quench Dynamics of Bosons in an Optical Lattice, Phys. Rev. Lett. **109**, 020505 (2012).

[62] D. A. Abanin and E. Demler, Measuring Entanglement Entropy of a Generic Many-Body System with a Quantum Switch, Phys. Rev. Lett. **109**, 020504 (2012).

[63] H.-C. Jiang, Z.-H. Wang, and L. Balents, Identifying topological order by entanglement entropy, Nat. Phys. **8**, 902 (2012).

[64] R. Islam, R. Ma, P. M. Preiss, M. E. Tai, A. Lukin, M. Rispoli, and M. Greiner, Measuring entanglement entropy in a quantum many-body system, Nature (London) **528**, 77 (2015).

[65] T. J. Osborne and M. A. Nielsen, Entanglement, quantum phase transitions, and density matrix renormalization, Quantum Inf. Process. **1**, 45 (2002).

[66] S. Sachdev, *Quantum Phase Transitions* (Cambridge University Press, Cambridge, 1999).

[67] P. Calabrese and J. Cardy, Entanglement entropy and quantum field theory, J. Stat. Mech. (2004) P06002.

[68] G. Vidal, J. Latorre, E. Rico, and A. Kitaev, Entanglement in Quantum Critical Phenomena, Phys. Rev. Lett. **90**, 227902 (2003).

[69] P. Calabrese and J. Cardy, Entanglement entropy and conformal field theory, J. Phys. A: Math. Theor. **42**, 504005 (2009).

[70] A. E. B. Nielsen, G. Sierra, and J. I. Cirac, Violation of the area law and long-range correlations in infinite-dimensional-matrix product states, Phys. Rev. A **83**, 053807 (2011).

[71] S.-J. Gu, Fidelity approach to quantum phase transitions, Int. J. Mod. Phys. B **24**, 4371 (2010).

[72] M. Hohenadler, Z. Y. Meng, T. C. Lang, S. Wessel, A. Muramatsu, and F. F. Assaad, Quantum phase transitions in the Kane-Mele-Hubbard model, Phys. Rev. B **85**, 115132 (2012).

[73] A. P. Gottlob and M. Hasenbusch, Critical behaviour of the 3D XY-model: A Monte Carlo study, Phys. A (Amsterdam) **201**, 593 (1993).

[74] A. Gaenko, A. Antipov, G. Carcassi, T. Chen, X. Chen, Q. Dong, L. Gamper, J. Gukelberger, R. Igarashi, S. Iskakov, M. Konz, J. LeBlanc, R. Levy, P. Ma, J. Paki, H. Shinaoka, S. Todo, M. Troyer, and E. Gull, Updated core libraries of the ALPS project, Comput. Phys. Commun. **213**, 235 (2017).

[75] B. Bauer, L. D. Carr, H. G. Evertz, A. Feiguin, J. Freire, S. Fuchs, L. Gamper, J. Gukelberger, E. Gull, S. Guertler, A. Hehn, R. Igarashi, S. V. Isakov, D. Koop, P. N. Ma, P. Mates, H. Matsuo, O. Parcollet, G. Pawłowski, J. D. Picon *et al.*, The ALPS project release 2.0: Open source software for strongly correlated systems, J. Stat. Mech.: Theory Exp. (2011) P05001.